Nacre-Inspired Multi-Scale Surface Architectures for Toughening Ceramic-Polymer Laminates

H. Yazdani Sarvestani[1]*, E. Azad[1,2], B. Ashrafi[1], M. Rahmat[3], M. Genest[4], F. Shadmehri[2], M. Hojjati[2]
[1]Aerospace Manufacturing Technology Center, National Research Council Canada, Montreal, QC H3T 2B2, Canada
[2]Concordia Center for Composites, Department of Mechanical, Industrial, and Aerospace Engineering, Concordia University, Montreal, QC H3G 1M8, Canada
[3]Aerospace Manufacturing Technologies Center, National Research Council Canada, Ottawa, ON, K1A 0R6, Canada
[4]Structures and Materials Performance Laboratory, National Research Council Canada, Ottawa, ON, K1A 0R6, Canada
* Corresponding author (Hamidreza.Yazdani@nrc-cnrc.gc.ca)

Keywords: *Hierarchical surface patterning; Ceramic–polymer laminates; Laser micromachining; Impact resistance; Cohesive-zone modelling*

1. Abstract

Brittle ceramics exhibit high stiffness, hardness, and thermal stability, but their limited fracture tolerance restricts their use in protective and aerospace structures subjected to repeated impact. Inspired by hierarchical biological armors, this work investigates a programmable laser micromachining strategy for toughening ceramic-polymer composite laminates through coordinated macro- and micro-scale surface architectures. Alumina-Surlyn® laminates were fabricated in four configurations: unpatterned Plain, micro-patterned (MP), hexagonal macro-patterned (Hex), and combined MP-Hex. Full-depth hexagonal cuts were introduced to steer cracks and promote tile-level segmentation, while shallow diagonal grooves were introduced to increase ceramic-polymer interfacial area and mechanical interlocking. Low-velocity impact tests, repeated low-energy impacts, zinc-iodide-enhanced X-ray radiography, double lap joint experiments, and cohesive-zone finite element simulations were used to link structural impact response with interface-level mechanics. The MP-Hex architecture achieved the highest absorbed energy under 20 J impact, with approximately 48% improvement relative to Plain laminates, while maintaining more stable stiffness and force capacity under repeated 2 J impacts. Double lap joint tests showed that micro-patterning increased average interfacial shear strength from about 11 MPa to about 18 MPa. The results demonstrate that surface patterning can control failure pathways across both the ceramic phase and the ceramic-polymer interface, providing a scalable route toward multi-hit-capable ceramic composite systems.

2. Introduction

Natural armors such as nacre, abalone shells, and mantis shrimp dactyl clubs combine stiff mineral constituents with soft interfaces to produce unusual combinations of stiffness, toughness, and damage tolerance [1-4]. A central design principle in these systems is hierarchical energy dissipation: cracks are not simply prevented, but redirected, bridged, arrested, or spread over a larger damage zone. Translating these principles to engineering ceramics is attractive because monolithic ceramics are strong and stiff, yet often fail through unstable crack growth under impact [5,6]. Ceramic-polymer laminates offer one route to overcoming this limitation by combining stiff ceramic layers with compliant polymer interlayers that can absorb energy, transfer load, and delay catastrophic fracture [7,8].

Previous bioinspired ceramic systems have demonstrated that macro-scale segmentation, interlocking tiles, stochastic architectures, and compliant interfaces can improve energy absorption and multi-hit response [5-9]. However, many designs emphasize either the geometry of the ceramic phase or the chemistry and roughness of the interface. The combined effect of surface-confined micro-patterns and through-thickness macro-patterns remains less understood, particularly under dynamic and repeated impact conditions. This is important because the ceramic-polymer interface is a critical failure location: weak adhesion promotes delamination, whereas stronger interfaces can redistribute shear stresses and force cracks to propagate through more energy-consuming pathways.

This conference paper condenses the main findings from a broader experimental-numerical study on programmable multi-scale surface architectures in alumina-Surlyn® laminates. The objective is to show how picosecond-laser micromachining can integrate two complementary mechanisms in one laminate: (i) shallow micro-grooves for interfacial strengthening and (ii) full-depth hexagonal segmentation for crack deflection and bridging. The paper further connects impact performance with double lap joint (DLJ) interface testing and cohesive-zone finite element analysis (FEA), thereby providing a mechanics-based interpretation of how multi-scale patterning improves damage tolerance.

3. Materials and Methods

3.1. *Laminate materials and surface architectures*

The rigid phase consisted of square alumina ceramic tiles with a nominal size of 114 × 114 mm², a thickness of 635 µm, and a density of 3875 kg/m³. Alumina was selected because of its high hardness, stiffness, wear resistance, and suitability for protective applications. The compliant phase was a 100 µm Surlyn® thermoplastic film used as the interlayer. Surlyn® was selected because ionomeric polymers can provide strong adhesion to ceramic surfaces while undergoing large-strain deformation and ligament formation during fracture.

Four laminate architectures were prepared. The Plain configuration contained unpatterned alumina plies laminated with Surlyn® interlayers. The MP configuration contained shallow diagonal grooves of about 20 µm depth and 200 µm width, intended to increase contact area and promote mechanical interlocking. The Hex configuration contained full-depth hexagonal cuts through the ceramic tiles, with a 5 mm side length, to segment the ceramic layer and promote crack deflection. The MP-Hex configuration combined both micro- and macro-patterns. All specimens used a nominal four-ply alumina stack with three Surlyn® interlayers, giving a total thickness of approximately 2.84 mm.

Table 1. Laminate configurations and intended toughening mechanisms.

Configuration	Surface architecture	Primary design function	Expected failure-control mechanism
Plain	No engineered pattern	Baseline response	Localized brittle cracking and delamination
MP	Shallow diagonal micro-grooves	Interface strengthening	Improved adhesion, shear transfer, and delayed debonding
Hex	Full-depth hexagonal segmentation	Structural crack steering	Crack deflection, tile movement, and crack bridging
MP-Hex	Combined micro- and macro-patterns	Hierarchical toughening	Synergistic interface retention and controlled crack propagation

3.2. *Laser micromachining and lamination*

An Ytterbium picosecond fiber laser was used to machine both scales of patterning. The micro-patterns were produced using a single pass at 24 W and a scan speed of 20 mm/s, while the hexagonal macro-patterns required 50 W, 17 mm/s, and 25 passes to reach full tile penetration. Wobble-assisted circular scanning was used to improve edge smoothness and repeatability. The patterned tiles and Surlyn® films were then stacked in an alternating arrangement, vacuum-bagged, and heat-treated at 146 °C for five hours. For the four-layer system, two tile designs with offset alignments were arranged in an ABAB sequence to reduce direct pattern overlap and promote distributed load transfer.

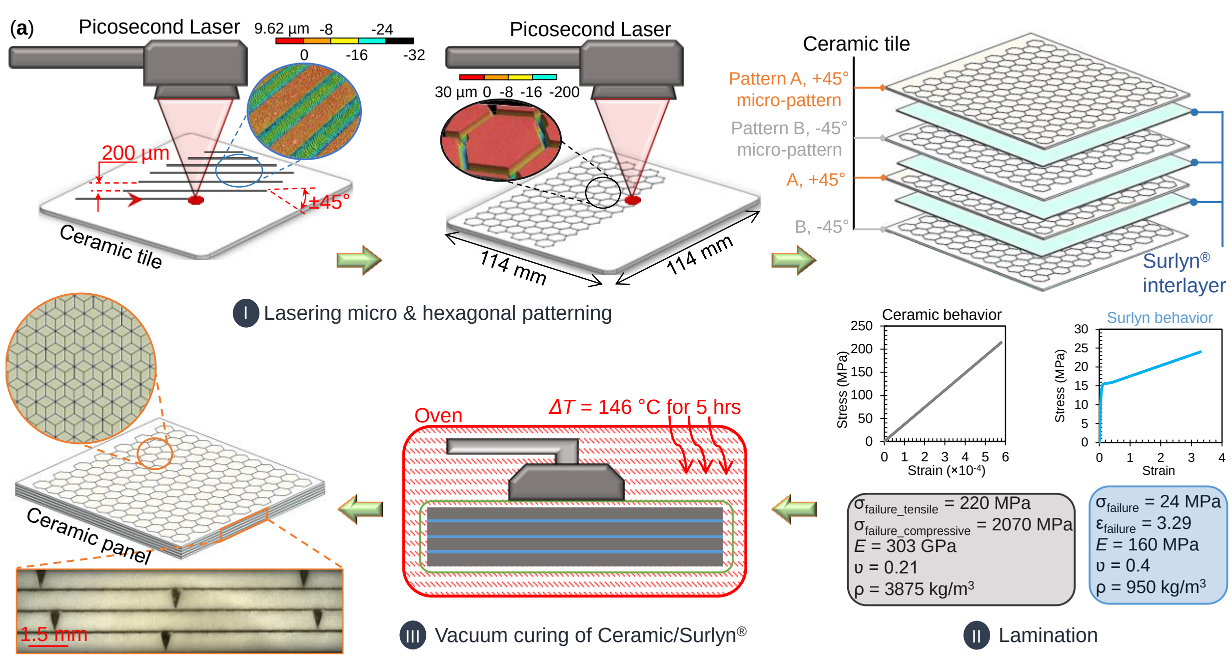

Figure 1. Representative manufacturing and characterization route for the patterned ceramic-polymer laminates: laser micromachining, lamination with Surlyn® interlayers, and verification of surface topography and polymer infiltration into micro-patterned grooves.

3.3. *Impact, damage visualization, and interface testing*

High-energy low-velocity impact tests were performed at 20 J using a drop tower with a 16 mm hemispherical impactor and a 76 mm clamped fixture. To evaluate damage accumulation without immediate perforation, repeated low-energy impacts were also performed at 2 J at two diagonally separated locations. Force-displacement and energy-time responses were used to evaluate stiffness, maximum reaction force, absorbed energy, and rebound behavior. Rebound percentage was used as a comparative indicator of elastic recovery and was calculated as:

$$\text{Rebound Percentage} = \left(\frac{\Delta_{max}-\Delta_{final}}{\Delta_{max}}\right)\times 100\% \qquad (1)$$

where Δ_{max} is the maximum impact displacement and Δ_{final} is the residual displacement after unloading. Standard X-ray radiography and zinc-iodide-enhanced X-ray radiography were used to visualize cracks and delamination. The radiopaque penetrant infiltrated debonded regions and fine cracks, thereby increasing contrast in the radiographs. To isolate interface mechanics, DLJ specimens were tested under displacement control. The average interfacial shear strength was calculated as τ = F/A, where F is the maximum load and A is the overlap area.

3.4. *Finite element modeling*

Three-dimensional FEA was conducted in ABAQUS to interpret the DLJ tests. Alumina and Garolite end-tabs were modeled with C3D8R elements, while the Surlyn® adhesive layer was represented using COH3D8 cohesive elements. The force-displacement response from DLJ experiments was used to calibrate the traction-separation behavior of the alumina-Surlyn® interface. Damage initiation was represented using a quadratic nominal stress criterion, and damage evolution was linked to the experimental damage dissipated energy. This approach enabled comparison between Plain and MP interfaces in terms of crack initiation, propagation rate, and mode II strain energy release behavior.

4. Results and Discussion

4.1. *Pattern quality and interface function*

Laser micromachining produced two distinct but complementary surface features. The full-depth hexagonal cuts segmented the ceramic layer and introduced predesigned crack-redirection paths, while the shallow micro-patterns preserved the global stiffness of the ceramic plies but modified the interface. Optical and laser scanning microscopy confirmed that Surlyn® infiltrated the shallow grooves, providing direct evidence of mechanical interlocking. This feature is important because it transforms the interface from a relatively planar adhesion surface into a patterned load-transfer zone. As a result, shear stresses are distributed over a larger effective area, and crack initiation at the ceramic-polymer boundary is delayed.

4.2. *Single-hit impact response at 20 J*

The 20 J impact tests showed that surface architecture strongly influenced stiffness, failure displacement, and absorbed energy. Plain and MP specimens exhibited similar initial stiffness values, indicating that shallow micro-grooves did not substantially reduce the bending stiffness of the laminate. In contrast, Hex and MP-Hex specimens showed lower initial stiffness because full-depth cuts segmented the ceramic layers and allowed earlier localized deformation. This stiffness reduction is a trade-off associated with structural segmentation; however, it also enables greater compliance and energy dissipation during impact.

All patterned configurations improved impact energy absorption relative to Plain laminates. The MP specimen reached the largest displacement before failure, which indicates a more distributed damage mode and improved load transfer through the interlayer. The Hex configuration promoted crack bridging and crack steering along tile boundaries. The combined MP-Hex design provided the most balanced response: micro-patterning strengthened the interface and delayed delamination, while hexagonal segmentation redirected cracks and increased crack path tortuosity. The MP-Hex design achieved the highest absorbed energy, approximately 48% greater than the Plain baseline.

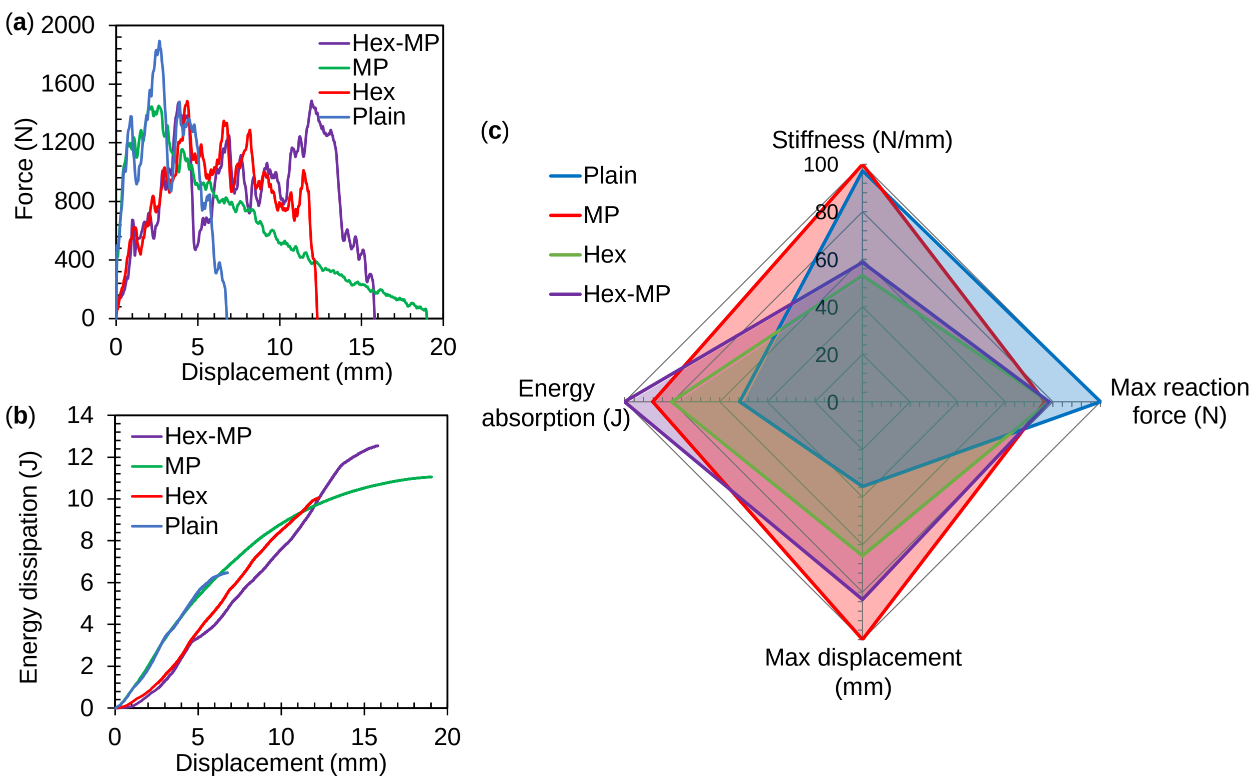

Figure 2. Mechanical response of Plain, MP, Hex, and MP-Hex laminates under 20 J low-velocity impact. Patterning modifies stiffness, maximum reaction force, failure displacement, absorbed energy, and post-impact fracture morphology.

4.3. *Repeated impact behavior and internal damage evolution*

Repeated 2 J impacts revealed differences in damage tolerance that were less visible in perforating 20 J tests. The Plain configuration absorbed nearly all of the input energy as irreversible damage, showing limited rebound and substantial stiffness degradation after the second impact. The Hex configuration improved the first-impact response, but the isolated macro-pattern was less effective after cumulative damage because interface-level delamination remained significant. In contrast, MP and MP-Hex specimens retained more stable force-displacement responses, with less reduction in stiffness and maximum force between the first and second impacts.

Zinc-iodide-enhanced radiography confirmed that micro-patterning suppressed interfacial delamination. Plain and Hex laminates showed larger bright regions associated with penetrant-filled cracks and debonded interfaces, while MP and MP-Hex laminates showed more localized damage. The MP-Hex configuration exhibited the most confined damage field, indicating that simultaneous control of interfacial adhesion and ceramic crack path can improve multi-hit resilience. These results support the interpretation that hierarchical patterning changes the dominant failure mode from localized brittle fracture and delamination to distributed cracking with partial elastic recovery.

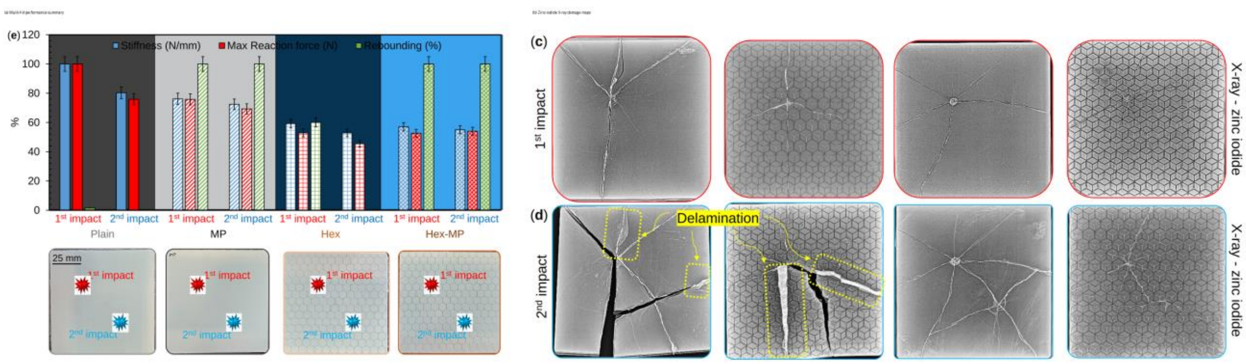

Figure 3. Repeated-impact performance and internal damage visualization. Patterned laminates, especially MP-Hex, retained greater rebound/stiffness stability and showed more localized zinc-iodide-enhanced X-ray damage signatures.

4.4. *Interface mechanics and cohesive-zone interpretation*

DLJ testing quantified the effect of micro-patterning on interfacial strength. Plain specimens showed an average interfacial shear strength of about 11 MPa, whereas MP specimens reached about 18 MPa. This increase is consistent with improved mechanical interlocking and larger effective contact area in the patterned interface. The failure mode also changed: Plain interfaces showed earlier adhesion-dominated failure, while MP interfaces exhibited stronger cohesive resistance associated with plastic deformation of the Surlyn® interlayer.

The cohesive-zone FE model reproduced the experimental force-displacement trends and clarified the damage evolution process. Both Plain and MP specimens initially behaved elastically, but Plain interfaces showed faster damage propagation after initiation. MP specimens sustained load transfer over a larger displacement range and reached a higher damage dissipated energy before complete debonding. The numerical results therefore support the experimental conclusion that micro-patterning does not merely roughen the surface; it changes the mechanics of the interface by delaying crack growth and increasing the effective mode II energy required for separation.

The overall energy absorption can be interpreted as the sum of elastic deformation, ceramic cracking, and interfacial delamination:

$$U_{total} = U_{elastic} + U_{crack} + U_{delam} \qquad (2)$$

where $U_{elastic}$ = ½ $k\Delta_f^2$ represents the elastic energy stored up to failure, with k as the effective stiffness and Δ_f as the failure displacement, defined as the strain at failure multiplied by the laminate thickness, $U_{crack} = A_{crack}G_c$ accounts for the energy consumed by tile cracking, with A_{crack} representing the total crack surface area and G_c the fracture energy (J/m^2), and $U_{delam} = A_{int}G_{int}$ represents the interfacial energy dissipation, dependent on delaminated area A_{int} and interfacial fracture energy G_{int}. In this framework, micro-patterning primarily increases the interfacial contribution by raising the energy required for delamination, whereas hexagonal patterning increases the crack-related contribution by lengthening and redirecting the ceramic crack path. The combined MP-Hex architecture is therefore effective because it acts at both length scales simultaneously: it delays interface failure and forces structural cracks into more tortuous, energy-consuming trajectories.

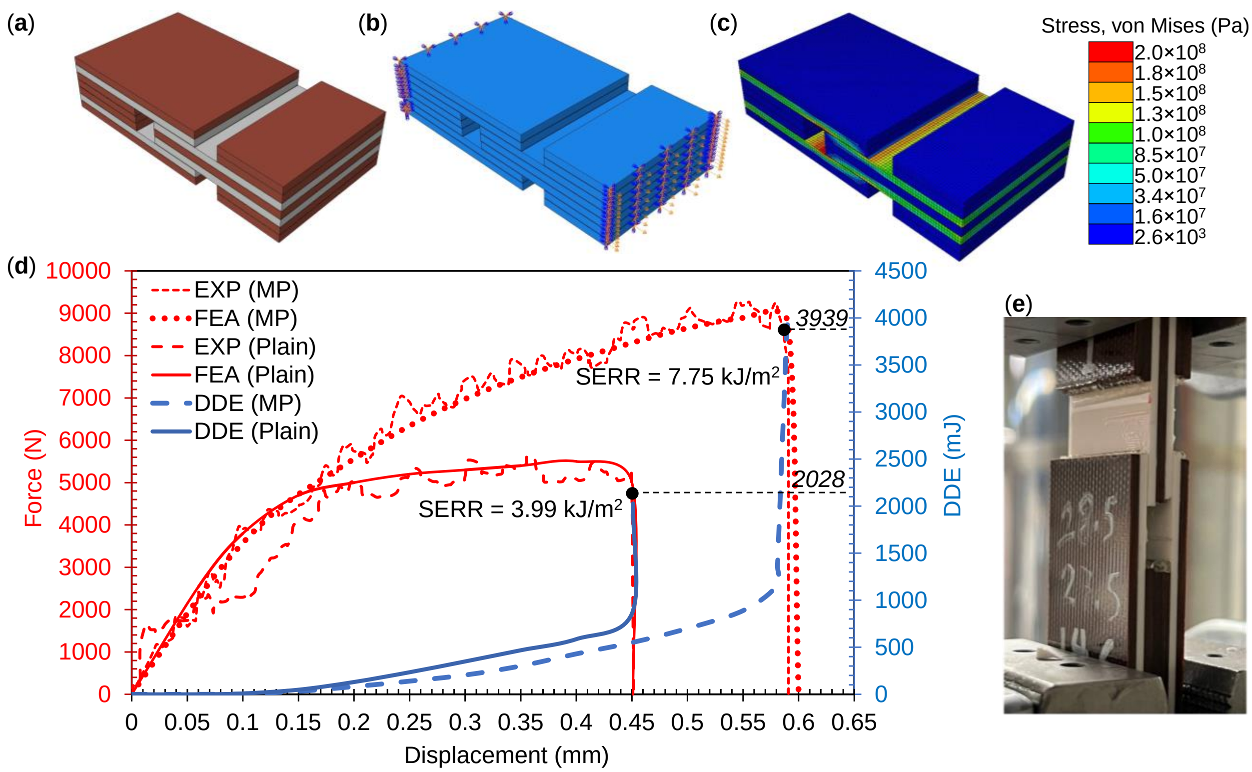

Figure 4. Experimental-numerical interface characterization using DLJ testing and cohesive-zone FEA. Micro-patterned interfaces show delayed damage propagation and higher dissipated energy than Plain interfaces.

5. Conclusions

Picosecond-laser micromachining was successfully used to reproducibly integrate shallow micro-patterns and full-depth hexagonal macro-patterns into alumina-Surlyn® ceramic-polymer laminates. The results showed that micro-patterning improved the ceramic-polymer interface by increasing the interfacial shear strength from approximately 11 MPa to 18 MPa, promoting Surlyn® infiltration into the laser-engraved grooves, and reducing delamination under impact loading. In parallel, hexagonal macro-patterning enhanced crack steering and bridging by segmenting the brittle ceramic layer, although this full-depth segmentation also reduced the initial stiffness of the laminate. Among all configurations, the combined MP-Hex architecture provided the most effective damage-tolerance response, achieving approximately 48% higher absorbed energy than Plain laminates under 20 J impact and maintaining more stable mechanical performance under repeated 2 J impacts. Cohesive-zone finite element simulations further confirmed that micro-patterned interfaces delay damage propagation and increase the energy required for mode II interfacial debonding. Overall, these findings demonstrate that the integration of micro-scale interfacial strengthening and macro-scale crack-guiding architectures offers a scalable and effective strategy for designing impact-resistant and multi-hit-capable ceramic composite systems for protective, aerospace, and extreme-environment applications.

Acknowledgment

Financial support from the National Research Council Canada (NRC) and the Natural Sciences and Engineering Research Council of Canada (NSERC) is gratefully acknowledged.

References

[1] F. Barthelat, H. Tang, P.D. Zavattieri, C.-M. Li and H.D. Espinosa. “On the mechanics of mother-of-pearl: a key feature in the material hierarchical structure”. Journal of the Mechanics and Physics of Solids, Vol. 55, pp. 306-337, 2007.
[2] U.G.K. Wegst, H. Bai, E. Saiz, A.P. Tomsia and R.O. Ritchie. “Bioinspired structural materials”. Nature Materials, Vol. 14, pp. 23-36, 2015.
[3] A. Ghazlan, T. Ngo, P. Tan, Y.M. Xie, P. Tran and M. Donough. “Inspiration from Nature's body armours - A review of biological and bioinspired composites”. Composites Part B: Engineering, Vol. 205, 108513, 2021.
[4] R.P. Behera and H. Le Ferrand. “Impact-resistant materials inspired by the mantis shrimp's dactyl club”. Matter, Vol. 4, pp. 2831-2849, 2021.
[5] H.Y. Sarvestani, M. Mirkhalaf, A. Akbarzadeh, D. Backman, M. Genest and B. Ashrafi. “Multilayered architectured ceramic panels with weak interfaces: energy absorption and multi-hit capabilities”. Materials & Design, Vol. 167, 107627, 2019.
[6] H.Y. Sarvestani, D. Aranguren van Egmond, I. Esmail, M. Genest, C. Paquet and B. Ashrafi. “Bioinspired stochastic design: tough and stiff ceramic systems”. Advanced Functional Materials, Vol. 32, 2108492, 2022.
[7] H.Y. Sarvestani, I. Esmail, Z. Katz, S. Jain, J. Sa, D. Backman and B. Ashrafi. “Interlocking design, programmable laser manufacturing and testing for architectured ceramics”. Scientific Reports, Vol. 12, 17330, 2022.
[8] A. Rahimizadeh, H.Y. Sarvestani, L. Li, J.B. Robles, D. Backman, L. Lessard and B. Ashrafi. “Engineering toughening mechanisms in architectured ceramic-based bioinspired materials”. Materials & Design, Vol. 198, 109375, 2021.
[9] E. Azad, H.Y. Sarvestani, B. Ashrafi, F. Shadmehri and M. Hojjati. “From macro to micro: bioinspired designs for tougher ceramics”. Journal of Materials Research and Technology, Vol. 31, pp. 3310-3319, 2024.
[10] C. Beausoleil, H.Y. Sarvestani, Z. Katz, J. Gholipour and B. Ashrafi. “Deep and high precision cutting of alumina ceramics by picosecond laser”. Ceramics International, Vol. 46, pp. 15285-15296, 2020.
[11] I. Esmail, H.Y. Sarvestani, J. Gholipour and B. Ashrafi. “Engineered net shaping of alumina ceramics using picosecond laser”. Optics & Laser Technology, Vol. 135, 106669, 2021.

[12] R. Chen, J. Liu, C. Yang, D.A. Weitz, H. He, D. Li, D. Chen, K. Liu and H. Bai. "Transparent impact-resistant composite films with bioinspired hierarchical structure". ACS Applied Materials & Interfaces, Vol. 11, pp. 23616-23622, 2019.

[13] F. Sun, C. Pruncu, P. Penchev, J. Jiang, S. Dimov and B. Blackman. "Influence of surface micropatterns on the mode I fracture toughness of adhesively bonded joints". International Journal of Adhesion and Adhesives, Vol. 103, 102718, 2020.

[14] Y. Wang, G. Zheng, N. Jiang, G. Ying, Y. Li, X. Cai, J. Meng, L. Mai, M. Guo and Y.S. Zhang. "Nature-inspired micropatterns". Nature Reviews Methods Primers, Vol. 3, 68, 2023.

[15] T. Lacelle, K.L. Sampson, H.Y. Sarvestani, A. Rahimizadeh, J.B. Robles, M. Mirkhalaf, M. Rafiee, M.B. Jakubinek, C. Paquet and B. Ashrafi. "Additive manufacturing of polymer derived ceramics: Materials, methods, and applications". APL Materials, Vol. 11, 2023.

[16] ASTM D7136/D7136M. "Standard Test Method for Measuring the Damage Resistance of a Fiber-Reinforced Polymer Matrix Composite to a Drop-Weight Impact Event". ASTM International.

[17] ASTM D3763. "Standard Test Method for High Speed Puncture Properties of Plastics Using Load and Displacement Sensors". ASTM International.